ACS APPLIED MATERIALS & INTERFACES

Research Article

www.acsami.org

Biocompatible Green and Red Fluorescent Organic Dots with Remarkably Large Two-Photon Action Cross Sections for Targeted Cellular Imaging and Real-Time Intravital Blood Vascular Visualization

Jiayun Xiang,[†] Xiaolei Cai,[§] Xiaoding Lou,[∥] Guangxue Feng,[§] Xuehong Min,[∥] Wenwen Luo,[‡] Bairong He,[‡] Chi Ching Goh,[⊥] Lai Guan Ng,[⊥] Jian Zhou,[†] Zujin Zhao,*[,†,‡] Bin Liu,*[,§] and Ben Zhong Tang*[,‡,#]

[†]College of Material, Chemistry and Chemical Engineering, Hangzhou Normal University, Hangzhou 310036, China

[‡]State Key Laboratory of Luminescent Materials and Devices, South China University of Technology, Guangzhou 510640, China

[§]Department of Chemical and Biomolecular Engineering, National University of Singapore, Singapore 117585

[∥]School of Chemistry and Chemical Engineering, Huazhong University of Science and Technology, Wuhan 430074, China

[⊥]Singapore Immunology Network (SIgN), A*STAR (Agency for Science Technology and Research), Biopolis 138648, Singapore

[#]Department of Chemistry, The Hong Kong University of Science & Technology, Clear Water Bay, Kowloon, Hong Kong 999077, China

Supporting Information

ABSTRACT: Fluorescent organic dots are emerging as promising bioimaging reagents because of their high brightness, good photostability, excellent biocompatibility, and facile surface functionalization. Organic dots with large two-photon absorption (TPA) cross sections are highly desired for two-photon fluorescence microscopy. In this work, we report two biocompatible and photostable organic dots fabricated by encapsulating tetraphenylethene derivatives within DSPE-PEG matrix. The two organic dots show absorption maxima at 425 and 483 nm and emit green and red fluorescence at 560 and 645 nm, with high fluorescence quantum yields of 64% and 22%, respectively. Both organic dots exhibit excellent TPA property in the range of 800−960 nm, affording upon excitation at 820 nm remarkably large TPA cross sections of 1.2×10^6 and 2.5×10^6 GM on the basis of dot concentration. The bare fluorophores and their organic dots are biocompatible and have been used to stain living cells for one- and two-photon fluorescence bioimagings. The cRGD-modified organic dots can selectively target integrin $\alpha_v\beta_3$ overexpressing breast cancer cells for targeted imaging. The organic dots are also applied for real-time two-photon fluorescence in vivo visualization of the blood vasculature of mouse ear, providing the spatiotemporal information about the whole blood vascular network. These results demonstrate that the present fluorescent organic dots are promising candidates for living cell and tissue imaging.

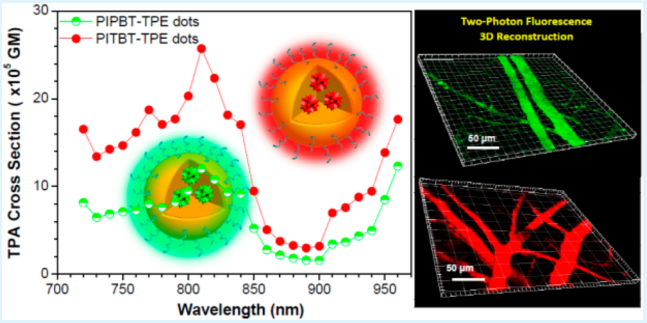

KEYWORDS: *organic dots, two-photon absorption, two-photon fluorescence, bioimaging, tetraphenylethene*

INTRODUCTION

Two-photon fluorescence (TPF) microscopy is a highly promising noninvasive technology for living cell and tissue imaging, which shows increased penetration depth, higher spatiotemporal resolution, diminished tissue autofluorescence interference, and reduced photodamage as compared to one-photon imaging.[1−5] The excitation lights used for TPF technology are usually in the near-infrared (NIR) region (700−1000 nm) to which the water and blood are nearly transparent and nonscattering. Hence, the contrast agents should possess large two-photon absorption (TPA) cross sections (δ) in this NIR region for TPF microscopy. In addition, high fluorescence quantum yields (Φ) of the contrast agents are also desirable for high-contrast TPF images. The two-photon action cross section is determined as the product of $\delta\Phi$,[6] and a large $\delta\Phi$ value is beneficial to increase the quality of the images and reduce the demand on equipment.

Recently, there has been strong motivation and great endeavor to develop fluorescent organic dots for biomedical applications such as targeted bioimaging[7−11] because of their distinct advantages, including lower cytotoxicity than inorganic quantum dots[12−14] and higher photobleaching resistance than

Received: May 2, 2015
Accepted: June 21, 2015
Published: June 21, 2015

DOI: 10.1021/acsami.5b03766
ACS Appl. Mater. Interfaces 2015, 7, 14965−14974

molecular probes such as fluorescent proteins[15−17] and small organic dyes.[18−21] These organic dots are comprised of organic fluorophores as the emitting core and biocompatible/biodegradable polymers as the encapsulation matrix, and they can enter the targeted cells easily via an endocytosis process.[22−25] Surface functionalization can be readily carried out on organic dots to endow them with high selectivity and specificity and to improve their solubility and stability in aqueous environments as well. Organic dots for TPF microscopy applications have been extensively studied, whose δ values are envisioned to reach a higher level simply by increasing the amount of organic fluorophores encapsulated.[26−28] The approach shows the merit of avoiding the complicated synthetic procedures to enlarge the δ value of organic molecules, but may encounter a new problem of fluorescence quenching as many common fluorophores show aggregation-caused quenching in solid state.

To solve this problem, a novel photophysical phenomenon of aggregation-induced emission (AIE)[29−31] has drawn researchers' attention. The emissions of AIE-active molecules are enhanced rather than weakened during the aggregation process, affording high fluorescence efficiencies in nanoparticles and solid films. Preliminary results have shown that fluorescent organic dots for TPF bioimaging application are achievable by encapsulating organic fluorophores within the polymeric matrix.[32−38] To further develop organic dots with excellent TPA properties, tunable emission wavelengths, and high emission efficiencies, in this work we designed and synthesized two fluorophores for the fabrication of organic dots for TPF bioimaging application (Figure 1). Both molecules have an

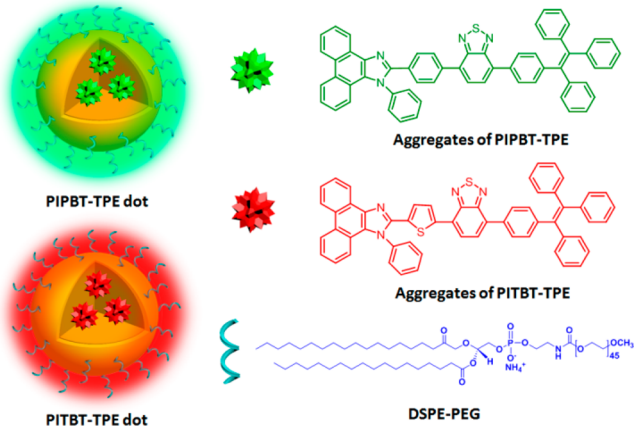

Figure 1. Schematic illustration of organic dots based on PIPBT-TPE and PITBT-TPE.

electron donor−acceptor (D−A) framework but with distinct green and red fluorescence. Tetraphenylethene (TPE),[32,39−42] a famous AIE archetype, is used as functional group to alleviate the emission-quenching effect caused by the strong dipole−dipole interactions of D−A molecules during the dot fabrication process. The DSPE-PEG encapsulated organic dots were fabricated and show high Φ values up to 64% and large δ values up to 2.5×10^6 GM (1 GM = 1×10^{-50} cm^4 s photon^{-1} molecule^{-1}) per dot upon excitation at 820 nm. Both dots perform well in TPF imaging of targeted cancer cells and real-time intravital visualization of the blood vasculature of mouse ear.

RESULTS AND DISCUSSION

The new TPE derivatives, PIPBT-TPE and PITBT-TPE, were synthesized in good yields according to the synthetic routes illustrated in Scheme S1. Detailed synthetic procedures and characterization data are described in the Supporting Information. Both fluorophores can be molecularly dissolved in THF and DMSO but are insoluble in water. To improve water solubility, stability, and selectivity of PIPBT-TPE and PITBT-TPE for bioimaging, fluorescent organic dots based on their aggregates were formulated by a modified nanoprecipitation method using 1,2-distearoyl-*sn*-glycero-3-phosphoethanolamine-*N*-[methoxy(polyethylene glycol)-2000 (DSPE-PEG) as the encapsulation matrix (Figure 1).[26,43] The average hydrodynamic diameters of the organic dots of PIPBT-TPE and PITBT-TPE were determined to be ∼45 and ∼40 nm, respectively, by dynamic light scattering (DLS; Figure 2). The high-resolution transmission electron microscopy (HR-TEM) images reveal spherical morphologies with mean diameters of ∼40 and ∼35 nm (insets, Figure 2) for PIPBT-TPE dots and PITBT-TPE dots, respectively. As shown in Figures S1 and S2, there are no obvious changes in the particle size and zeta potential in 4 weeks, and no aggregation and precipitation was observed for PIPBT-TPE dots and PITBT-TPE dots in aqueous solutions after being stored at 4 °C for several months, all of which indicate the good stability of the dots.

As illustrated in Figure 3A, in THF solution PIPBT-TPE shows an absorption maximum at 418 nm and green photoluminescence (PL) at 550 nm, whereas PITBT-TPE absorbs much longer wavelengths at 476 and emits red PL at 598 nm. Although the structural difference between PIPBT-TPE and PITBT-TPE is small, the absorption and PL spectra of PITBT-TPE are greatly bathochromically shifted relative to those of PIPBT-TPE, which is mainly caused by the stronger intramolecular charge transfer (ICT) originating from the better electron-donating ability of the thiophene group than the phenyl ring.[44] PIPBT-TPE and PITBT-TPE in THF solutions show good TPA properties in the range of ∼750−850 nm, with maxima δ values of 120 and 325 GM per fluorophore molecule, respectively, at an excitation wavelength of 810 nm (Figure S3). Most fluorophores that bear TPE moiety are weakly fluorescent in solutions because the active intramolecular rotation (IMR) process of the TPE moiety can effectively deactivate the excited state in a nonradiative manner.[30,31] PIPBT-TPE and PITBT-TPE, however, are highly emissive in THF solutions, giving excellent Φ values of 81 and 84%, respectively. Owing to the low energy level of benzo-2,1,3-thiadiazole moiety, the lowest unoccupied molecular orbitals (LUMOs) of PIPBT-TPE and PITBT-TPE are mainly localized on this moiety, whereas the TPE moiety shows no contribution to the LUMOs, as revealed by the theory calculation (Figure 4). The highest occupied molecular orbitals (HOMOs), however, are extended obviously along the whole conjugated backbones, but the TPE moiety shows relatively small contribution. These electronic structures imply that the IMR process of the TPE moiety becomes ineffective in quenching the excited states of PIPBT-TPE and PITBT-TPE, rendering high Φ values of the molecules in the solution state.[36,40,44]

The absorption maxima of PIPBT-TPE dots and PITBT-TPE dots are located at 425 and 483 nm, respectively, which are close to those in THF solutions (Table 1). The emission peaks of PIPBT-TPE dots and PITBT-TPE dots are centered at

DOI: 10.1021/acsami.5b03766
ACS Appl. Mater. Interfaces 2015, 7, 14965−14974

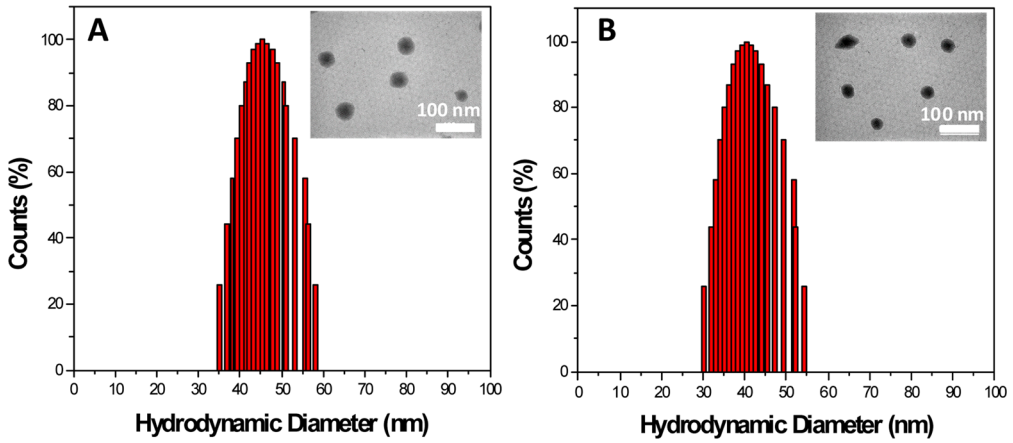

Figure 2. DLS results of (A) PIPBT-TPE dots and (B) PITBT-TPE dots; insets, HR-TEM images of the dots.

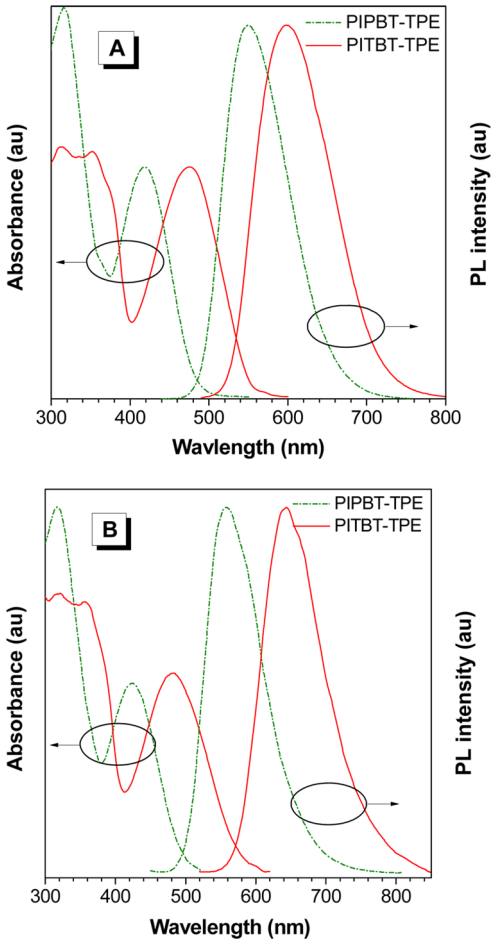

Figure 3. Absorption and PL spectra of PIPBT-TPE and PITBT-TPE (A) in THF solutions and (B) in dots in aqueous solutions.

560 and 645 nm. Large Stokes shifts of 135 and 162 nm are found for PIPBT-TPE dots and PITBT-TPE dots, respectively, which can minimize the background interference and are favored in bioimaging applications (Figure 3B). In comparison with the PL in THF solution, the PL of PITBT-TPE dots exhibits a bathochromic shift of 47 nm, which is much larger than that of PIPBT-TPE dots (10 nm). The Φ values of PIPBT-TPE dots and PITBT-TPE dots in aqueous solutions were determined to be 64 and 22%, using 4-(dicyanomethylene)-2-methyl-6-[4-(dimethylaminostyryl)-4H-pyran] (DCM) in methanol as the reference (43%). The Φ value of PITBT-TPE dots decreases greatly relative to that in solution, whereas the Φ value of PIPBT-TPE dots shows a smaller drop. The larger decrease in emission efficiency and stronger bathochromic shift in emission wavelength of PITBT-TPE versus PIPBT-TPE dots should be attributed to that the PITBT-TPE molecules undergo stronger intermolecular dipole−dipole interactions in the aggregated state because of their stronger ICT effect and larger dipole moment (Figure 4).

The TPA spectra of PIPBT-TPE dots and PITBT-TPE dots in aqueous solutions were investigated by TPA imaging microscopy in the wavelength range of 800−960 at 10 nm intervals. Figure 5 indicates that the maximum δ values of PIPBT-TPE dots and PITBT-TPE dots are 1.2×10^6 and 2.5×10^6 GM (based on dot concentration) at an excitation wavelength of 820 nm, resulting in $\Phi\delta$ values of 7.7×10^5 and 5.6×10^5 GM, respectively, calculated by using Rhodamine 6G in methanol as the reference. The values of δ and $\Phi\delta$ are much higher than those of widely used commercial dyes, such as Evans Blue, and other nanoparticles in the literature.[26,28,38,45−47] These results indicate that PIPBT-TPE dots and PITBT-TPE dots are promising luminescent reagents for TPA imaging.

Before evaluating the actual performance of the dots, the one- and two-photon fluorescence bioimaging applications of the bare fluorophores were tested. As shown in Figure 6A,B, strong red fluorescence is recorded from the cytoplasmic regions of HeLa cells upon incubation with PITBT-TPE in DMSO solution (10 μg mL^{-1}) for 2 h and excitation at 488 nm. Similar fluorescence images are also obtained upon excitation at 980 nm (Figure 6C,D), indicative of the great potential for TPF imaging. PIPBT-TPE in DMSO solution also shows good ability to stain cytoplasm of HeLa cells, and bright-green fluorescence is observed under excitation at 405 nm (Figure S4A,B). However, when excited at 980 nm, the fluorescence signal is hardly collected (Figure S4C,D), owing to the weak TPA of PIPBT-TPE at such long wavelength. In view of this, the red-fluorescent PITBT-TPE is more advantageous than green-fluorescent PIPBT-TPE for TPF imaging. Both PIPBT-TPE and PITBT-TPE show low cytotoxicity, as revealed by methylthiazolyldiphenyltetrazolium bromide (MTT) assays to evaluate the metabolic viability of HeLa cells after incubation with PIPBT-TPE or PITBT-TPE in DMSO at varied concentrations (Figure S5). These results demonstrate that

DOI: 10.1021/acsami.5b03766
ACS Appl. Mater. Interfaces 2015, 7, 14965−14974

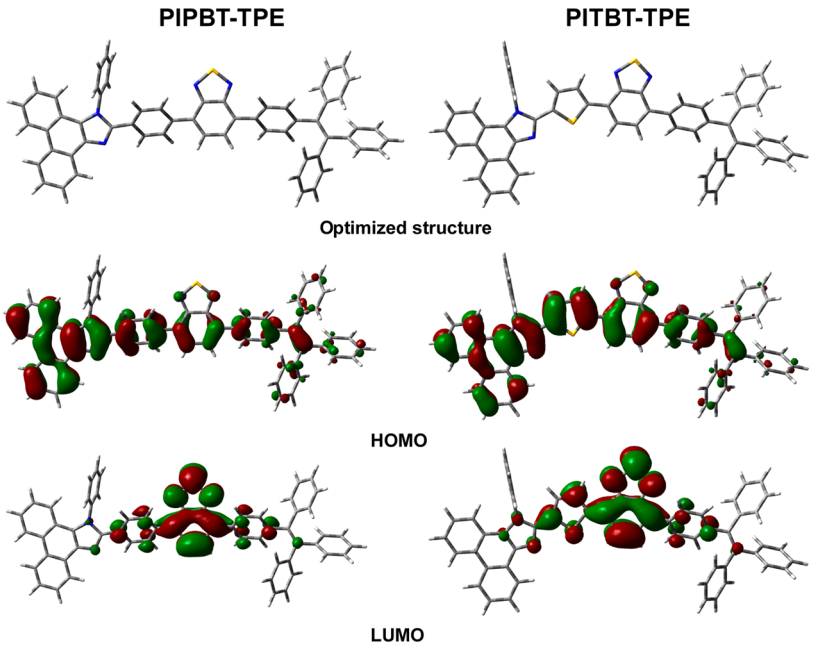

Figure 4. Optimized molecular structures and molecular orbital amplitude plots of HOMOs and LUMOs of PIPBT-TPE and PITBT-TPE calculated using the B3LYP/6-31G(d) basis set.

Table 1. Optical Properties of PIPBT-TPE and PITBT-TPE in THF and in Dots

	THF				dots			
	λ_{abs} (nm)	λ_{em} (nm)	Φ (%)[a]	δ (GM)	λ_{abs} (nm)	λ_{em} (nm)	Φ (%)[b]	δ (× 10^6, GM)
PIPBT-TPE	418	550	81	120	425	560	64	1.2
PITBT-TPE	476	598	84	325	483	645	22	2.5

[a]Determined using an integrating sphere. [b]Determined using DCM in methanol as the reference (Φ = 43%).

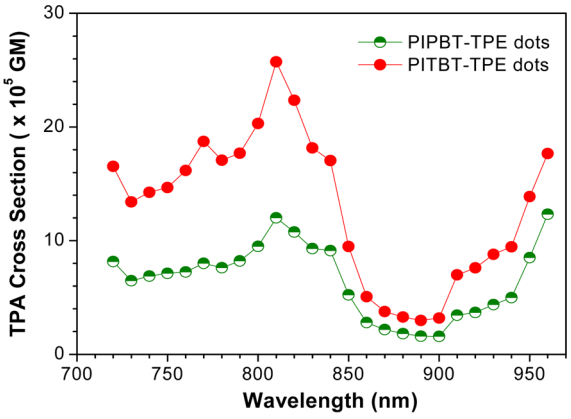

Figure 5. Two-photon absorption (TPA) spectra of PIPBT-TPE dots and PITBT-TPE dots in aqueous solutions.

PIPBT-TPE and PITBT-TPE themselves are biocompatible and can directly stain cells for fluorescence bioimaging.

The one- and two-photon fluorescence bioimaging applications of PIPBT-TPE dots and PITBT-TPE dots were further investigated. To improve the cancer-cell specificity of both dots, cyclic arginine-glycine-aspartic acid (cRGD) tripeptide, which could target integrin $\alpha_v\beta_3$ overexpressing cancer cells, was further conjugated to the surface of the dots for targeted cancer cell imaging.[48] Using (1,2-distearoyl-*sn*-glycero-3-phosphoethanolamine-*N*-[maleimide(polyethylene glycol)-2000]) (lipid-PEG-Mal) as the matrix, followed by click reaction with thiol-functionalized cRGD, the obtained dots have a high concentration of cRGD on the surface. Cell imaging was conducted by incubating MDA-MB-231, an integrin $\alpha_v\beta_3$ overexpressing breast cancer cell line, and normal NIH/3T3 mouse cell line for 4 h in cell culture medium with 2 nM PIPBT-TPE-cRGD and PITBT-TPE-cRGD dots at 37 °C. The cells were further costained with a nucleic acid stain, 4′,6-diamidino-2-phenylindole (DAPI), to localize the distribution of dots in the cell. Confocal images illustrated in Figures 7 and 8 reveal that MDA-MB-231 cells display strong green or red fluorescence from cell cytoplasm, whereas almost no fluorescence from the cytoplasm of NIH/3T3 cells but only blue fluorescence at the nucleus generated by DAPI could be observed, indicating that both dots could selectively target integrin $\alpha_v\beta_3$ overexpressing breast cancer cells for targeted imaging.

TPF microscope imaging of MDA-MB-231 cells was further studied with an excitation wavelength at 800 nm, and the emission was collected using a 580−760 nm bandpass filter. As shown in Figure 9, the cytoplasm could be clearly distinguished and cell morphology is readily discerned by the strong fluorescence, proving that PIPBT-TPE-cRGD and PITBT-TPE-cRGD dots are promising TPF probes for cell imaging. The cytotoxicity of PIPBT-TPE-cRGD and PITBT-TPE-cRGD dots was also investigated by using MTT assays through evaluation of the metabolic viability of MDA-MB-231 breast cancer cells after incubation with both dots at various concentrations and time. Figure 10 shows the cell viability after incubation with the dots suspension at 1, 5, and 10 μM

DOI: 10.1021/acsami.5b03766
ACS Appl. Mater. Interfaces 2015, 7, 14965−14974

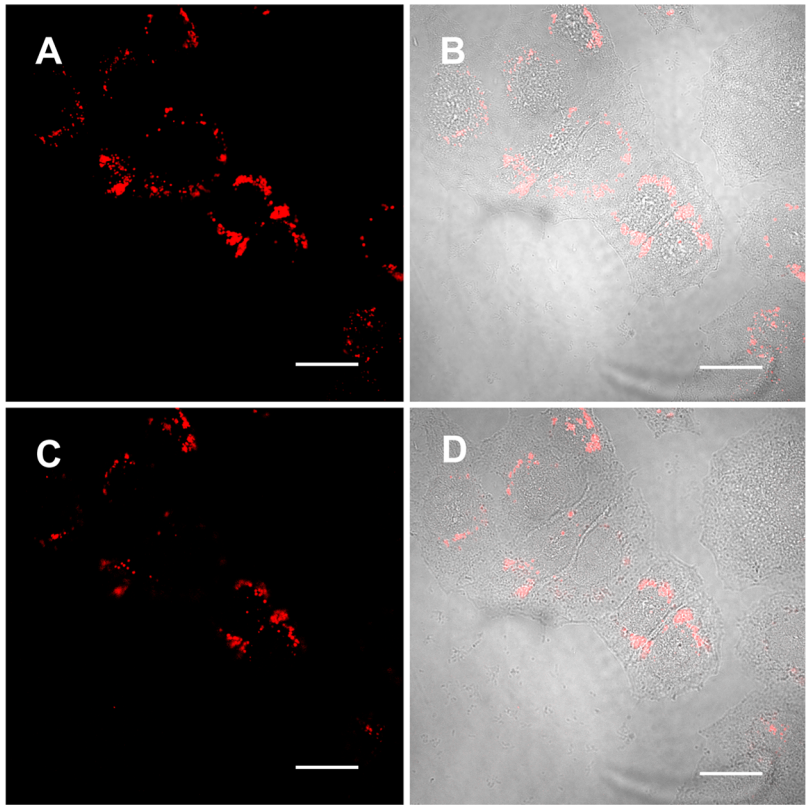

Figure 6. Confocal images of HeLa cells stained by PITBT-TPE dissolved in DMSO solution (10 μg mL^{-1}). The images were obtained upon excitation at (A) 488 nm and (C) 980 nm, and the fluorescence was collected through a 570−620 nm bandpass filter. (B and D) Merged images of corresponding bright-field images with panels A and C, respectively. All the images share the same scale bar of 20 μm.

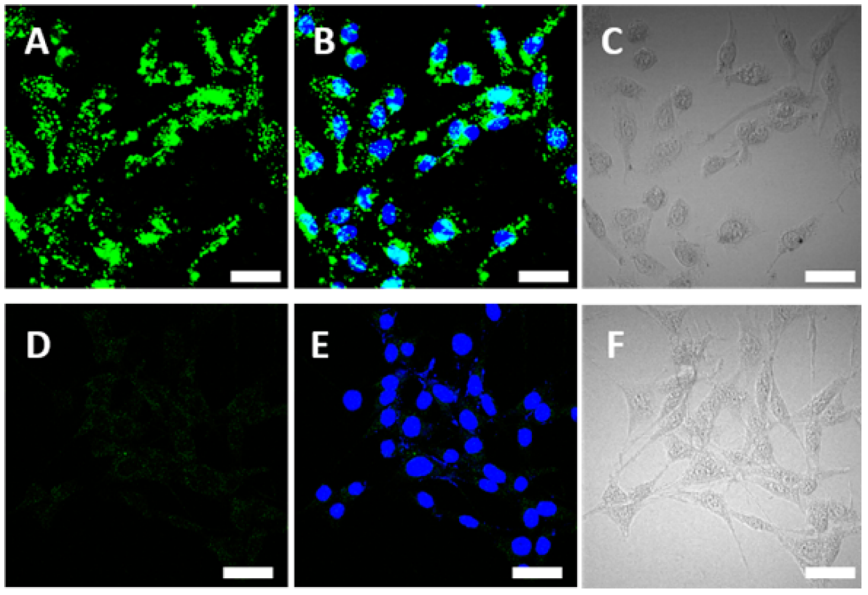

Figure 7. Confocal images of (A and B) MDA-MB-231cells and (D and E) NIH/3T3 cells labeled by PIPBT-TPE-cRGD dots upon excitation at 405 nm. (C and F) Corresponding bright-field images. The nuclei were stained by DAPI (λ_{ex} = 358 nm, λ_{em} = 461 nm). All the images share the same scale bar of 40 μm.

dye concentrations for 24, 48, and 72 h, respectively. The high cell viability indicates the good biocompatibility of the dots.

Meanwhile, the photostability of the PIPBT-TPE dots and PITBT-TPE dots was also evaluated by comparing the fluorescence intensity at various time points in the MDA-MB-231 cancer cells with initial fluorescence intensity after continuous scanning. Generally, both kinds of dots show pretty good photostability, which indicates their ability for biological fluorescence imaging. Close survey of the results discloses that PIPBT-TPE dots show almost no decrease in emission intensity, but the emission intensity of PITBT-TPE dots drops by ∼25% upon continuous laser excitation at 800 nm for

DOI: 10.1021/acsami.5b03766
ACS Appl. Mater. Interfaces 2015, 7, 14965−14974

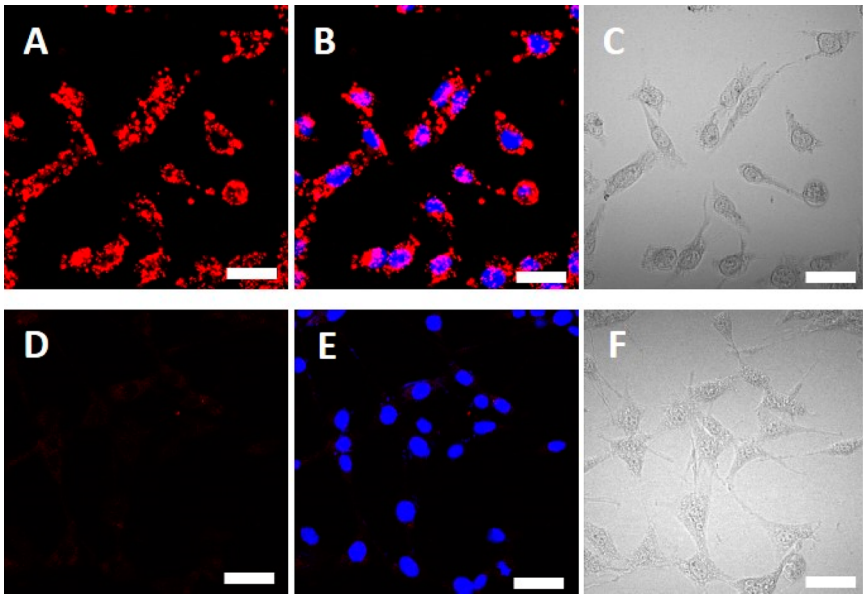

Figure 8. Confocal images of (A and B) MDA-MB-231cells and (D and E) NIH/3T3 cells labeled by PITBT-TPE-cRGD dots upon excitation at 488 nm. (C and F) Corresponding bright-field images. The nuclei are stained by DAPI (λ_{ex} = 358 nm, λ_{em} = 461 nm). All the images share the same scale bar of 40 μm.

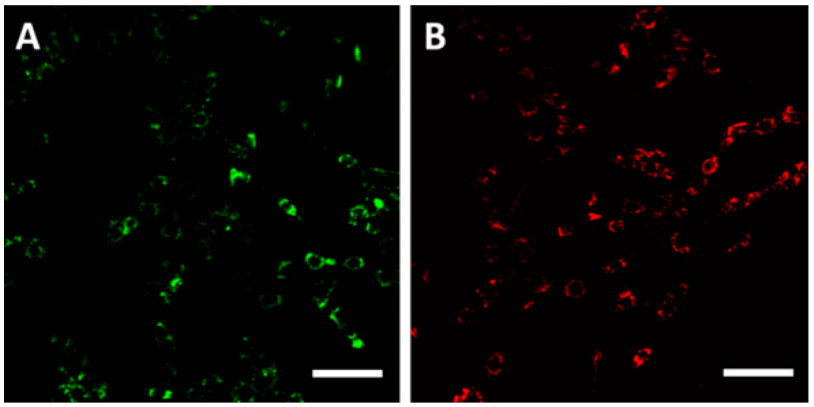

Figure 9. Two-photon fluorescence images of MDA-MB-231 cancer cells treated with (A) PIPBT-TPE-cRGD dots and (B) PITBT-TPE-cRGD dots. All the images share the same scale bar of 100 μm.

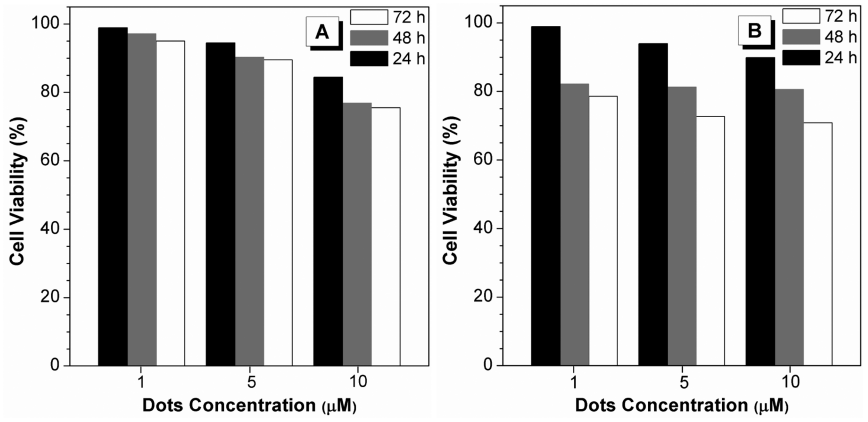

Figure 10. Viability of MDA-MB-231 cells after incubation with (A) PIPBT-TPE-cRGD dots and (B) PITBT-TPE-cRGD dots for 24, 48, and 72 h at different concentrations.

10 min (Figure 11), demonstrating that the PIPBT-TPE dots have higher photostability than PITBT-TPE dots. This is probably due to the fact that the phenyl ring is more tolerant with photooxidization than thiophene moiety.

DOI: 10.1021/acsami.5b03766
ACS Appl. Mater. Interfaces 2015, 7, 14965−14974

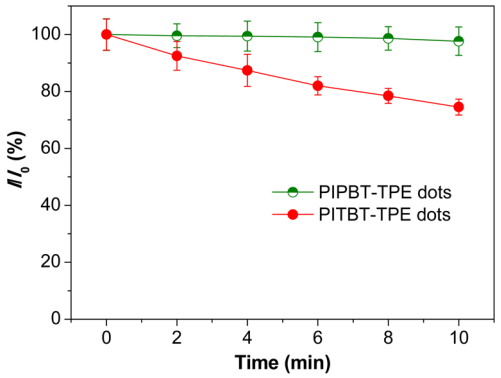

Figure 11. Photostability of PIPBT-TPE dots and PITBT-TPE dots in MDA-MB-231 cancer cells upon continuous laser excitation at 800 nm. I_0 is the initial fluorescence intensity, and I is the fluorescence intensity at various time points after continuous scanning.

The applicability of PIPBT-TPE dots and PITBT-TPE dots for real-time in vivo two-photon fluorescence imaging was further studied by TPF imaging microscopy. In vivo imaging of the blood vasculature of mouse ear was conducted using both dots as the blood vessel visualizing agents. Figure 12 displays the 3D reconstructions, Z-projected images that demonstrate the overall blood vasculature, as well as the distinct blood vasculature at different depths. It is obvious that the blood vascular network including the major blood vasculature, small capillaries, and even arteries located deeply over 80 μm could be visualized, providing spatiotemporal information about the whole blood vascular network. After injection of PIPBT-TPE or PITBT-TPE dots, continuous and smooth blood flows with bright-green or red fluorescence can be clearly observed in blood vessels (Figure S6) without obvious aggregates throughout 30 min, indicating the excellent stability and biocompatibility of PIPBT-TPE dots and PITBT-TPE dots in a living biological system.

CONCLUSIONS

Two TPE derivatives with efficient green and red fluorescence are synthesized and utilized to prepare organic dots by encapsulation within DSPE-PEG matrix. The generated organic dots show high fluorescence efficiency and remarkably large TPA cross section values. The bare fluorophores in DSMO solutions and their organic dots in aqueous media can be used as luminescent reagents for TPF imaging for living cells with good biocompatibility and high photostability, and the organic dots carrying cRGD groups at the surface can selectively target integrin $\alpha_v\beta_3$ overexpressing breast cancer cells for imaging. Both organic dots also serve well in real-time two-photon intravital blood vascular imaging of the mouse ear skin. These results demonstrate the great potential of the present green and red fluorescent organic dots in TPF bioimaging applications.

EXPERIMENTAL SECTION

Preparation of PIPBT-TPE Dots and PITBT-TPE Dots. PIPBT-TPE dots and PITBT-TPE dots were prepared using a modified nanoprecipitation method.[21,35] A 1 mL volume of THF solution containing 1 mg of DSPE-PEG and 0.5 mg of PIPBT-TPE or PITBT-TPE was mixed with 10 mL of Milli-Q water and immediately sonicated using a microtip probe sonicator (XL2000, Misonix Incorporated, NY) at 12 W output for 60 s. The mixture was then stirred overnight at room temperature to evaporate THF. The solution was then filtered by a 200 nm syringe filter and concentrated by centrifugation.

Synthesis of PIPBT-TPE-cRGD Dots and PITBT-TPE-cRGD Dots. PIPBT-TPE-Mal and PITBT-TPE-Mal dots were first prepared using the same method by replacing DSPE-PEG with DSPE-PEG-Mal. Then, 3.6 μL of thiol-functionalized cRGD (0.1 M, DMSO) was added into 5 mL of PIPBT-TPE-Mal or PITBT-TPE-Mal dots suspension solution. The mixtures were stirred overnight at room temperature. The obtained solutions were dialyzed by 12 000−14 000 kDa

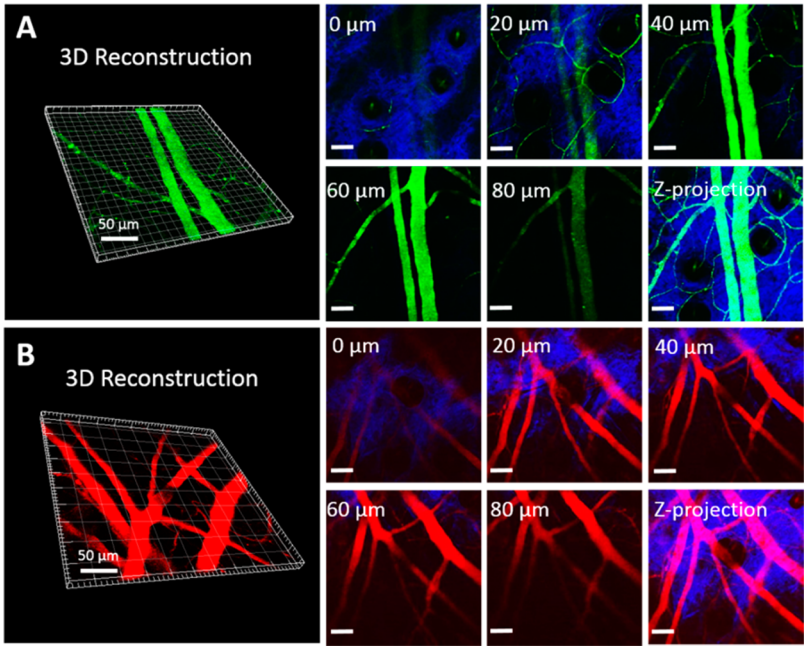

Figure 12. Two-photon fluorescence images of ear blood vessels stained with (A) PIPBT-TPE dots and (B) PITBT-TPE dots, including 3D-reconstructed images of blood vessels, images at different vertical depths of mouse ear, and Z-projection images. All the images share the same scale bar of 50 μm.

DOI: 10.1021/acsami.5b03766
ACS Appl. Mater. Interfaces 2015, 7, 14965−14974

membrane against Milli-Q water for 3 days in order to remove excess cRGD and DMSO.

Cell Culture and Imaging with PITBT-TPE and PIPBT-TPE Dissolved in DMSO. HeLa cancer cells were cultured in 1640 (GIBCO) medium with 10% fetal calf serum and 1% penicillin−streptomycin (PS, 10 000 IU penicillin and 10 000 μg mL^{-1} streptomycin, MULTICELL) in a culture flask at 37 °C in a humidified atmosphere with 5% CO_2. HeLa cells were grown overnight on a plasma-treated 20 mm round coverslip mounted onto a 35 mm Petri dish with an observation window. The living cells were stained with PITBT-TPE or PIPBT-TPE in DMSO (10 μg mL^{-1}) for 2 h. The data were acquired by OLYMPUS biological confocal laser scanning microscope (model: FV1200). For PITBT-TPE: excitation wavelength, 488 or 980 nm; emission collected, 570−620 nm. For PIPBT-TPE: Eexcitation wavelength, 405 or 980 nm; emission collected, 500−580 nm.

Cell Culture and Imaging with Organic Dots. MDA-MB-231 breast cancer cells and NIH/3T3 mouse cells were cultured in Dulbecco's modified Eagle's medium (DMEM) containing 10% FBS and 1% PS at 37 °C in a humidified environment containing 5% CO_2. The cells were precultured to reach confluence before experiments. MDA-MB-231 breast cancer cells and NIH/3T3 mouse cells were cultured in the 8-well confocal-imaging chambers at 37 °C. After reaching 80% confluence, the culture medium was removed and 1× PBS buffer was used to wash the adherent cells twice. PIPBT-TPE-cRGD dots or PITBT-TPE-cRGD dots in FBS-free DMEM medium were added into the wells. The cells were washed three times with 1× PBS buffer after incubation for 4 h. Then, the cells were further incubated with DAPI for 30 min and washed twice with 1× PBS buffer. One-photon fluorescence images of MDA-MB-231 breast cancer cells and NIH/3T3 were obtained by CLSM (Zeiss LSM 410, Jena, Germany) with imaging software (Fluoview FV1000). The signal of PIPBT-TPE-cRGD dots or PITBT-TPE-cRGD dots is collected above 505 nm upon excitation at 488 nm. The signal of DAPI is collected between 430 and 470 nm upon excitation at 405 nm. Two-photon fluorescence images of MDA-MB-231 breast cancer cells were acquired using a TriM Scope II single-beam two-photon microscope (LaVision BioTec) with a tunable 680−1080 nm laser (Coherent).

Cytotoxicity of PIPBT-TPE and PITBT-TPE Molecules. Viability of the cells was assayed using cell proliferation Kit I with the absorbance of 570 nm being detected using a PerkinElmer Victor plate reader. A total of 10 000 cells were seeded per well in a 96-well plate. After overnight culture, various concentrations of PIPBT-TPE or PITBT-TPE were added to the 96-well plate. After 24 h treatment, 100 μL of MTT solution was added to each well. After incubation by 4 h at 37 °C, 200 μL of DMSO was added. Then, the optical density readings at 570 nm were taken using a plate reader. Each experiment was performed by at least three times.

Cytotoxicity of PIPBT-TPE-cRGD Dots and PITBT-TPE-cRGD Dots. MTT assays were applied to assess the metabolic activity of MDA-MB-231 breast cancer cells. MDA-MB-231 cells were incubated in 96-well plates (Costar, IL, USA) at a concentration of 4×10^4 cells mL^{-1}. The culture medium was replaced by fresh culture medium with different concentrations of PIPBT-TPE-cRGD dots or PITBT-TPE-cRGD dots after 24 h incubation. The cells were further incubated for 24, 36, and 72 h, respectively. Then, the wells were washed three times with 1× PBS buffer, and 100 μL of MTT solution (0.5 mg mL^{-1}) was added into each well. After 3 h incubation, the MTT solution was carefully removed. DMSO (100 μL) was added into each well. To dissolve all the precipitates formed, the plate was shaken for 10 min gently at room temperature. A microplate reader (Genios Tecan) was used to measure the absorbance of MTT at 570 nm. Cell viability was calculated by the ratio of absolute absorbance of the cells incubated with dots suspension to that of the cells incubated with culture medium only.

Real-Time Two-Photon Intravital Blood Vascular Imaging of the Ear Skin. For two-photon imaging experiments, mice were first anesthetized using 150 mg kg^{-1} ketamine and 10 mg kg^{-1} xylazine and then placed on a heating pad to maintain their core body temperature throughout the imaging procedure. Before injection of PIPBT-TPE dots or PITBT-TPE dots, the hair on the ear skin is completely removed using hair removal cream. A 100 μL aliquot of 50 nM PIPBT-TPE dots or PITBT-TPE dots based on the dot concentration were administered via retro-orbital injection before imaging. The images were obtained by using a TriM Scope II single-beam two-photon microscope (LaVision BioTec) with a tunable 680−1080 nm laser (Coherent). All procedures were performed under the institution's IACUC (Institutional Animal Care and Use Committee) guidelines.

■ ASSOCIATED CONTENT

Ⓢ Supporting Information

General information, synthetic procedures (Scheme S1) and characterization data, dot concentration calculation, determinations of two-photon absorption cross sections, DLS size and zeta potential evolution of PIPBT-TPE dots and PITBT-TPE dots in 4 weeks (Figures S1 and S2), TPA spectra of PIPBT-TPE and PITBT-TPE in THF solutions (Figure S3), confocal images of HeLa cells stained by PIPBT-TPE dissolved in DMSO solution (Figure S4), spectra of viability of HeLa cells after incubation with PIPBT-TPE or PITBT-TPE in DMSO solution for 24 h at different concentrations (Figure S5), and two-photon images of blood vessels at mouse ear skin after injection of PIPBT-TPE dots and PITBT-TPE dots for 30 min (Figure S6). The Supporting Information is available free of charge on the ACS Publications website at DOI: 10.1021/acsami.5b03766.

■ AUTHOR INFORMATION

Corresponding Authors

*E-mail: mszjzhao@scut.edu.cn.
*E-mail: cheliub@nus.edu.sg.
*E-mail: tangbenz@ust.hk.

Author Contributions

J.X. and X.C. contributed equally to this work.

Notes

The authors declare no competing financial interest.

■ ACKNOWLEDGMENTS

We acknowledge the financial support from the National Natural Science Foundation of China (51273053, 21405054, and 21404029), the Guangdong Natural Science Funds for Distinguished Young Scholar (2014A030306035), the Guangdong Innovative Research Team Program of China (201101C0105067115) and the National Basic Research Program of China (973 Program, 2013CB834702), and Fundamental Research Funds for the Central Universities (2015PT020), and Singapore National Research Foundation (R279-000-444-281).

■ REFERENCES

(1) Larson, D. R.; Zipfel, W. R.; Williams, R. M.; Clark, S. W.; Bruchez, M. P.; Wise, F. W.; Webb, W. W. Water-Soluble Quantum Dots for Multiphoton Fluorescence Imaging in Vivo. *Science* **2003**, *300*, 1434−1436.

(2) Zipfel, W. R.; Williams, R. M.; Webb, W. W. Nonlinear Magic: Multiphoton Microscopy in the Biosciences. *Nat. Biotechnol.* **2003**, *21*, 1369−1377.

(3) Cahalan, M. D.; Parker, I.; Wei, S. H.; Miller, M. J. Two-photon Tissue Imaging: Seeing the Immune System in a Fresh Light. *Nat. Rev. Immunol.* **2002**, *2*, 872−880.

(4) He, G. S.; Tan, L. S.; Zheng, Q.; Prasad, P. N. Multiphoton Absorbing Materials: Molecular Designs, Characterizations, and Applications. *Chem. Rev.* **2008**, *108*, 1245−1330.

DOI: 10.1021/acsami.5b03766
ACS Appl. Mater. Interfaces 2015, 7, 14965−14974

(5) Helmchen, F.; Denk, W. Deep Tissue Two-Photon Microscopy. *Nat. Methods* **2005**, *2*, 932−940.
(6) He, F.; Tian, L. L.; Tian, X.; Xu, H.; Wang, Y.; Xie, W.; Hanif, M.; Xia, J.; Shen, F.; Yang, B.; Li, F.; Ma, Y.; Yang, Y.; Shen, J. Diphenylamine-Substituted Cruciform Oligo(phenylene vinylene): Enhanced One- and Two-Photon Excited Fluorescence in the Solid State. *Adv. Funct. Mater.* **2007**, *17*, 1551−1557.
(7) Ding, D.; Li, K.; Liu, B.; Tang, B. Z. Bioprobes Based on AIE Fluorogens. *Acc. Chem. Res.* **2013**, *46*, 2441−2453.
(8) Zhang, X.; Zhang, X.; Tao, L.; Chi, Z.; Xu, J.; Wei, Y. Aggregation Induced Emission-Based Fluorescent Nanoparticles: Fabrication Methodologies and Biomedical Applications. *J. Mater. Chem. B* **2014**, *2*, 4398−4414.
(9) Li, K.; Yamamoto, M.; Chan, S. J.; Chiam, M. Y.; Qin, W.; Wong, P. T. H.; Yim, E. K. F.; Tang, B. Z.; Liu, B. Organic Nanoparticles with Aggregation-Induced Emission for Tracking Bone Marrow Stromal Cells in the Rat Ischemic Stroke Model. *Chem. Commun.* **2014**, *50*, 15136−15139.
(10) Ding, D.; Kwok, R. T. K.; Yuan, Y.; Feng, G.; Tang, B. Z.; Liu, B. A Fluorescent Light-Up Nanoparticle Probe with Aggregation-Induced Emission Characteristics and Tumor-Acidity Responsiveness for Targeted Imaging and Selective Suppression of Cancer Cells. *Mater. Horiz.* **2015**, *2*, 100−105.
(11) Ma, C.; Ling, Q.; Xu, S.; Zhu, H.; Zhang, G.; Zhou, X.; Chi, Z.; Liu, S.; Zhang, Y.; Xu, J. Preparation of Biocompatible Aggregation-Induced Emission Homopolymeric Nanoparticles for Cell Imaging. *Macromol. Biosci.* **2014**, *14*, 235−243.
(12) Derfus, A. M.; Chan, W. C. W.; Bhatia, S. N. Probing the Cytotoxicity of Semiconductor Quantum Dots. *Nano Lett.* **2004**, *4*, 11−18.
(13) Lewinski, N.; Colvin, V.; Drezek, R. Cytotoxicity of Nanoparticles. *Small* **2008**, *4*, 26−49.
(14) Kirchner, C.; Liedl, T.; Kudera, S.; Pellegrino, T.; Muñoz Javier, A.; Gaub, H. E.; Stölzle, S.; Fertig, N.; Parak, W. J. Cytotoxicity of Colloidal CdSe and CdSe/ZnS Nanoparticles. *Nano Lett.* **2005**, *5*, 331−338.
(15) Chen, F. Q.; Gerion, D. Fluorescent CdSe/ZnS Nanocrystal−Peptide Conjugates for Long-Term, Nontoxic Imaging and Nuclear Targeting in Living Cells. *Nano Lett.* **2004**, *4*, 1827−1832.
(16) Jaiswal, J. K.; Goldman, E. R.; Mattoussi, H.; Simon, S. M. Use of Quantum Dots for Live Cell Imaging. *Nat. Methods* **2004**, *1*, 73−78.
(17) Shah, L. S.; Clark, P. A.; Moioli, E. K.; Stroscio, M. A.; Mao, J. J. Labeling of Mesenchymal Stem Cells by Bioconjugated Quantum Dots. *Nano Lett.* **2007**, *7*, 3071−3079.
(18) Liu, Y.; Kong, M.; Zhang, Q.; Zhang, Z.; Zhou, H.; Zhang, S.; Li, S.; Wu, J.; Tian, Y. A Series of Triphenylamine-Based Two-Photon Absorbing Materials with AIE Property for Biological Imaging. *J. Mater. Chem. B* **2014**, *2*, 5430−5440.
(19) Kim, H. J.; Heo, C. H.; Kim, H. M. Benzimidazole-Based Ratiometric Two-Photon Fluorescent Probes for Acidic pH in Live Cells and Tissues. *J. Am. Chem. Soc.* **2013**, *135*, 17969−17977.
(20) Yang, W.; Chan, P. S.; Chan, M. S.; Li, K. F.; Lo, P. K.; Mak, N. K.; Cheah, K. W. M.; Wong, S. Two-Photon Fluorescence Probes for Imaging of Mitochondria and Lysosomes. *Chem. Commun.* **2013**, *49*, 3428−3430.
(21) Capodilupo, A. L.; Vergaro, V.; Fabiano, E.; De Giorgi, M.; Baldassarre, F.; Cardone, A.; Maggiore, A.; Maiorano, V.; Sanvitto, D.; Gigli, G.; Ciccarella, G. Design and Synthesis of Fluorenone-Based Dyes: Two-Photon Excited Fluorescent Probes for Imaging of Lysosomes and Mitochondria in Living Cells. *J. Mater. Chem. B* **2015**, *3*, 3315−3323.
(22) Li, K.; Liu, B. Polymer-Encapsulated Organic Nanoparticles for Fluorescence and Photoacoustic Imaging. *Chem. Soc. Rev.* **2014**, *43*, 6570−6597.
(23) Zhang, X.; Zhang, X.; Wang, S.; Liu, M.; Zhang, Y.; Tao, L.; Wei, Y. Facile Incorporation of Aggregation-Induced Emission Materials into Mesoporous Silica Nanoparticles for Intracellular Imaging and Cancer Therapy. *ACS Appl. Mater. Interfaces* **2013**, *5*, 1943−1947.
(24) Feng, G.; Tay, C. Y.; Chui, Q. X.; Liu, R.; Tomczak, N.; Liu, J.; Tang, B. Z.; Leong, D. T.; Liu, B. Ultrabright Organic Dots with Aggregation-Induced Emission Characteristics for Cell Tracking. *Biomaterials* **2014**, *35*, 8669−8677.
(25) Ding, D.; Mao, D.; Li, K.; Wang, X.; Qin, W.; Liu, R.; Chiam, D. S.; Tomczak, N.; Yang, Z.; Tang, B. Z.; Kong, D.; Liu, B. Precise and Long-Term Tracking of Adipose-Derived Stem Cells and Their Regenerative Capacity via Superb Bright and Stable Organic Nanodots. *ACS Nano* **2014**, *8*, 12620−12631.
(26) Li, K.; Jiang, Y.; Ding, D.; Zhang, X.; Liu, Y.; Hua, J.; Feng, S.-S.; Liu, B. Folic Acid-Functionalized Two-Photon Absorbing Nanoparticles for Targeted Mcf-7 Cancer Cell Imaging. *Chem. Commun.* **2011**, *47*, 7323−7325.
(27) Wang, G.; Pu, K.-Y.; Zhang, X.; Li, K.; Wang, L.; Cai, L.; Ding, D.; Lai, Y.-H.; Liu, B. Star-Shaped Glycosylated Conjugated Oligomer for Two-Photon Fluorescence Imaging of Live Cells. *Chem. Mater.* **2011**, *23*, 4428−4434.
(28) Aparicio-Ixta, L.; Ramos-Ortiz, G.; Pichardo-Molina, J. L.; Maldonado, J. L.; Rodríguez, M.; Tellez-Lopez, V. M.; Martinez-Fong, D.; Zolotukhin, M. G.; Fomine, S.; Meneses-Nava, M. A.; Barbosa-García, O. Two-Photon Excited Fluorescence of Silica Nanoparticles Loaded with a Fluorene-Based Monomer and Its Cross-Conjugated Polymer: Their Application to Cell Imaging. *Nanoscale* **2012**, *4*, 7751−7759.
(29) Luo, J.; Xie, Z.; Lam, J. W. Y.; Cheng, L.; Chen, H.; Qiu, C.; Kwok, H. S.; Zhan, X.; Liu, Y.; Zhu, D.; Tang, B. Z. Aggregation-Induced Emission of 1-Methyl-1,2,3,4,5-pentaphenylsilole. *Chem. Commun.* **2001**, 1740−1741.
(30) Hong, Y.; Lam, J. W. Y.; Tang, B. Z. Aggregation-Induced Emission: Phenomenon, Mechanism and Applications. *Chem. Commun.* **2009**, 4332−4353.
(31) Hong, Y.; Lam, J. W. Y.; Tang, B. Z. Aggregation-Induced Emission. *Chem. Soc. Rev.* **2011**, *40*, 5361−5388.
(32) Zhao, Z.; Lam, J. W. Y.; Tang, B. Z. Tetraphenylethene: A Versatile AIE Building Block for the Construction of Efficient Luminescent Materials for Organic Light-Emitting Diodes. *J. Mater. Chem.* **2012**, *22*, 23726−23740.
(33) Gao, Y.; Feng, G.; Jiang, T.; Goh, C.; Ng, L.; Liu, B.; Li, B.; Yang, L.; Hua, J.; Tian, H. Biocompatible Nanoparticles Based on Diketo-Pyrrolo-Pyrrole (DPP) with Aggregation-Induced Red/NIR Emission for In Vivo Two-Photon Fluorescence Imaging. *Adv. Funct. Mater.* **2015**, *25*, 2857−2866.
(34) Jiang, T.; Qu, Y.; Li, B.; Gao, Y.; Hua, J. Tetraphenylethene End-Capped [1,2,5]Thiadiazolo[3,4-c]pyridine with Aggregation-induced Emission and Large Two-Photon Absorption Cross-Sections. *RSC Adv.* **2015**, *5*, 1500−1506.
(35) Ye, Q.; Chen, S.; Zhu, D.; Lu, X.; Lu, Q. Preparation of Aggregation-Induced Emission Dots for Long-Term Two-Photon Cell Imaging. *J. Mater. Chem. B* **2015**, *3*, 3091−3097.
(36) Zhao, Z.; Chen, B.; Geng, J.; Chang, Z.; Aparicio-Ixta, L.; Nie, H.; Goh, C. C.; Ng, L. G.; Qin, A.; Ramos-Ortiz, G.; Liu, B.; Tang, B. Z. Red Emissive Biocompatible Nanoparticles from Tetraphenylethene-Decorated BODIPY Luminogens for Two-Photon Excited Fluorescence Cellular Imaging and Mouse Brain Blood Vascular Visualization. *Part. Part. Syst. Charact.* **2014**, *31*, 481−491.
(37) Wang, D.; Qian, J.; Qin, W.; Qin, A.; Tang, B. Z.; He, S. Biocompatible and Photostable AIE Dots with Red Emission for *In Vivo* Two-Photon Bioimaging. *Sci. Rep.* **2014**, *4*, 4279.
(38) Qian, J.; Zhu, Z.; Qin, A.; Qin, W.; Chu, L.; Cai, F.; Zhang, H.; Wu, Q.; Hu, R.; Tang, B. Z.; He, S. High-Order Non-Linear Optical Effects in Organic Luminogens with Aggregation-Induced Emission. *Adv. Mater.* **2015**, *27*, 2332−2339.
(39) Zhao, Z.; Lam, J. W. Y.; Tang, B. Z. Aggregation-Induced Emission of Tetraarylethene Luminogens. *Curr. Org. Chem.* **2010**, *14*, 2109−2132.
(40) Zhao, Z.; Geng, J.; Chang, Z.; Chen, S.; Deng, C.; Jiang, T.; Qin, W.; Lam, J. W. Y.; Kwok, H. S.; Qiu, H.; Liu, B.; Tang, B. Z. A Tetraphenylethene-Based Red Luminophor for an Efficient Non-

DOI: 10.1021/acsami.5b03766
ACS Appl. Mater. Interfaces 2015, 7, 14965−14974

Doped Electroluminescence Device and Cellular Imaging. *J. Mater. Chem.* **2012**, *22*, 11018−11021.
(41) Huang, Y.; Hu, F.; Zhao, R.; Zhang, G.; Yang, H.; Zhang, D. Tetraphenylethylene Conjugated with a Specific Peptide as a Fluorescence Turn-On Bioprobe for the Highly Specific Detection and Tracing of Tumor Markers in Live Cancer Cells. *Chem. - Eur. J.* **2014**, *20*, 158−164.
(42) Xue, X.; Zhao, Y.; Dai, L.; Zhang, X.; Hao, X.; Zhang, C.; Huo, S.; Liu, J.; Liu, C.; Kumar, A.; Chen, W.-Q.; Zou, G.; Liang, X.-J. Spatiotemporal Drug Release Visualized through a Drug Delivery System with Tunable Aggregation-Induced Emission. *Adv. Mater.* **2014**, *26*, 712−717.
(43) Li, K.; Qin, W.; Ding, D.; Tomczak, N.; Geng, J.; Liu, R.; Liu, J.; Zhang, X.; Liu, H.; Liu, B.; Tang, B. Z. Photostable Fluorescent Organic Dots with Aggregation-Induced Emission (AIE Dots) for Noninvasive Long-Term Cell Tracing. *Sci. Rep.* **2013**, *3*, 1150.
(44) Zhao, Z.; Deng, C.; Chen, S.; Lam, J. W. Y.; Qin, W.; Lu, P.; Wang, Z.; Kwok, H. S.; Ma, Y.; Qiu, H.; Tang, B. Z. Full Emission Color Tuning in Luminogens Constructed from Tetraphenylethene, Benzo-2,1,3-thiadiazole and Thiophene Building Blocks. *Chem. Commun.* **2011**, *47*, 8847−8849.
(45) Liu, P.; Li, S.; Jin, Y.; Qian, L.; Gao, N.; Yao, S. Q.; Huang, F.; Xu, Q.-H.; Cao, Y. Red-Emitting DPSB-Based Conjugated Polymer Nanoparticles with High Two-Photon Brightness for Cell Membrane Imaging. *ACS Appl. Mater. Interfaces* **2015**, *7*, 6754−6763.
(46) Geng, J.; Goh, C. C.; Tomczak, N.; Liu, J.; Liu, R.; Ma, L.; Ng, L. G.; Gurzadyan, G. G.; Liu, B. Micelle/Silica Co-protected Conjugated Polymer Nanoparticles for Two-Photon Excited Brain Vascular Imaging. *Chem. Mater.* **2014**, *26*, 1874−1880.
(47) Xu, Z.; Liao, Q.; Wu, Y.; Ren, W.; Li, W.; Liu, L.; Wang, S.; Gu, Z.; Zhang, H.; Fu, H. Water-Miscible Organic J-Aggregate Nanoparticles as Efficient Two-Photon Fluorescent Nano-Probes for Bio-Imaging. *J. Mater. Chem.* **2012**, *22*, 17737−17743.
(48) Yuan, Y.; Liu, B. Self-Assembled Nanoparticles Based on PEGylated Conjugated Polyelectrolyte and Drug Molecules for Image-Guided Drug Delivery and Photodynamic Therapy. *ACS Appl. Mater. Interfaces* **2014**, *6*, 14903−14910.

DOI: 10.1021/acsami.5b03766
ACS Appl. Mater. Interfaces 2015, 7, 14965−14974